

# Determining CT Requirements for Generator and Transformer Protective Relays

Ritwik Chowdhury, Dale Finney, and Normann Fischer, *Schweitzer Engineering Laboratories, Inc.*  
Douglas Taylor, *Avista Utilities*

**Abstract**—Modern relays often have algorithms that enhance the security of elements that are otherwise susceptible to current transformer (CT) saturation. While both IEEE and IEC provide guidance on sizing CTs for protective relay applications, the similarities and differences between the two guides have generally been unclear. In addition, the CT sizing criteria ultimately depend on the relay design and application settings and have been difficult to establish.

In this paper, we provide insight into the similarities and differences in the IEEE and IEC CT sizing requirements for generator and transformer differential applications. We also discuss ways to prevent misapplying such guidance for protective relays involved in these applications. We consider CT models and compare the various models commonly available to laboratory test data to provide insight into the model parameters and confirm the model validity. Subsequently, we present a methodology for evaluating CT requirements for generator and transformer protective relays.

Finally, we use the CT models and methods in conjunction with sample generator and transformer differential elements to obtain easy-to-use CT requirements and setting guidance for secure protective relay application. We also provide application guidance for generator black starts. Considerations such as CT remanence are discussed. An application example is included in the appendix.

## I. INTRODUCTION

Differential relays use the principle of Kirchhoff's current law (e.g., 87G generator differential element) or ampere-turn balance (e.g., 87T transformer differential element) to compare currents from all current transformers (CTs) composing the differential zone. Any missing current is understood to be flowing into a fault. However, there are other mechanisms that produce erroneous differential current. These mechanisms include transformer inrush, transformer turns ratio error due to a tap changer, CT transient response, and steady-state errors from the CT and the relay. This paper focuses on CT saturation, which corresponds to the response of the CT during a power system transient. CT saturation is primarily a concern during external faults.

Both IEEE [1] and IEC [2] provide guidelines on CT selection for differential protection. References [1] and [2] describe and quantify CT transient response. They also recognize that a complete analysis of protection performance cannot focus on the CT alone.

Differential protection, in its most basic form, is implemented with a percentage-slope characteristic with a minimum pickup setting and one or more slope characteristics [1]. Security is provided by the slope setting, which works well for external faults during CT saturation. In the past, tools were

developed to help protection engineers analyze basic protection responses in the presence of CT saturation [3].

The latest generation of digital relays includes advanced algorithms that go beyond the traditional percent-slope characteristic. These algorithms provide improved security during external events, including the energization of an external transformer during a black start. However, it is no longer an easy task for a protection engineer to analyze the behavior of these differential algorithms during faults. This complicates the task of CT selection.

This paper describes a method used to develop CT selection criteria for one such advanced differential algorithm. An approach that considers the combined responses of both the CT and the differential algorithm is employed. The resulting criteria follow the conventions provided by the IEEE and IEC guides for CT sizing. The criteria also consider the impact of differential element settings. An application example is included in the appendix.

## II. IEEE AND IEC GUIDANCE

### A. CT Equivalent Circuit

The most recognized guidance for the application of CTs is provided by IEEE [1] and IEC [2]. Both start with the equivalent circuit of a CT shown in Fig. 1.

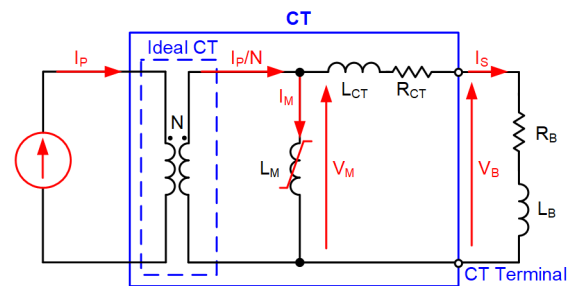


Fig. 1. Equivalent Circuit of a CT

$L_M$  is the non-linear magnetizing branch inductance, which can draw a large magnetizing current ( $I_M$ ). It corresponds to an error current for a differential relay that measures the secondary current ( $I_S$ ).  $I_P$  is the primary current,  $N$  is the CT turns ratio,  $V_M$  is the magnetizing branch voltage, and  $V_B$  is the burden voltage.

$R_{CT}$  is the CT internal resistance, and  $R_B$  is the burden resistance.  $L_{CT}$  is the CT leakage inductance, negligible for a toroidal CT.  $L_B$  is the burden inductance, neglected because digital relays do not have the same large inductive burden as electromechanical relays.

## B. IEEE Guidance

When there is a large fault current on the CT primary ( $I_p$ ), the core can saturate. Core saturation reduces  $L_M$  and increases  $I_M$ , which is an error quantity to the differential relay. The point-on-wave ( $\theta$ ) of fault inception determines the level of dc offset in the fault current and has a large influence on the degree of CT saturation. Most faults (95%) occur within 40 degrees of the voltage maximum [4]. While for the dominantly inductive power system this is favorable for CT performance (because it results in a reduced dc offset), providing CT application guidance requires consideration of the worst-case  $\theta$ .

To demonstrate the effect of  $\theta$ , in Fig. 2 we start with a no-offset and a fully offset fault current with a unity amplitude calculated by (1) and (2) for a 60 Hz system with a relatively low time constant ( $\tau$ ) of 30 ms ( $X/R$  ratio of 11.31). Using unity amplitude or a per-unit of the worst-case fault current dictated by the application (external faults in this case) facilitates simpler explanation of the concepts.

$$I_p = \sin(\omega t + \theta) - \sin(\theta) \cdot e^{-\frac{t}{\tau}} \quad (1)$$

$$\tau = \frac{1}{\omega} \cdot \left( \frac{X}{R} \right) \quad (2)$$

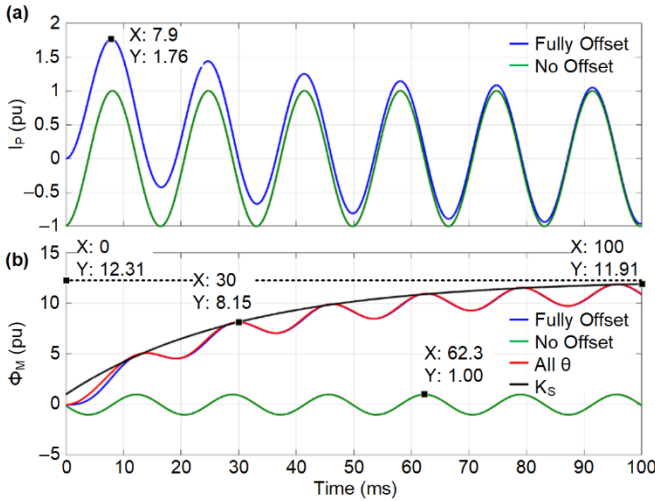


Fig. 2. Per-Unit Fault Current (a) and Excitation Flux (b) for a 60 Hz System With  $\tau = 30$  ms

In the linear operating region of the CT,  $I_M$  is minimal and the secondary current flows through the dominantly resistive secondary circuit. Assuming  $R_{CT} + R_B = 1$  pu for simplicity results in a per-unit  $V_M$  equal to  $I_p$ . When  $V_M$  is integrated and normalized, we obtain the per-unit CT core flux ( $\phi_M$ ) shown in (3) and (4).

$$\phi_M = -\cos(\omega t + \theta) + \frac{X}{R} \cdot \sin(\theta) \cdot e^{-\frac{t}{\tau}} + C \quad (3)$$

$$C = \cos(\theta) - \frac{X}{R} \cdot \sin(\theta) \quad (4)$$

$C$  is the constant of integration, and it forces the initial condition of  $\phi_M$  to 0. Fig. 2 shows that for a steady-state symmetrical fault current, if a CT were able to remain in the linear region for  $\phi_M$  greater than 1 pu, it would be enough to

avoid CT saturation. But, the decaying dc contributes significantly to the core flux and eventually stabilizes at a value of  $1 + X/R$ .

The IEEE guide introduces the concept shown in (5) of a saturation factor ( $K_S$ ). In (5),  $V_{SAT}$  is the saturation voltage of the CT defined at the magnetizing branch and can be obtained by inspecting an ANSI CT excitation curve where the excitation current is 10 A [1].  $K_S$  is the factor by which the CT is over-dimensioned with respect to a purely ac fault current ( $\theta = 0^\circ$ ). It is calculated as the ratio of the saturation voltage  $V_{SAT}$  to the expected  $V_M$  for a maximum symmetrical fault current [1]. If the CT is sized such that  $K_S$  is greater than  $1 + X/R$ , the CT will never saturate when there is no remanence; otherwise, it will saturate after some time [1].

$$K_S = \frac{V_{SAT}}{I_S \cdot (R_{CT} + R_B)} \quad (5)$$

IEEE provides (6) to calculate the concept of time to saturate ( $T_S$ ), assuming no pre-fault load current. For the purposes of protective relaying, modern differential relays (described in Section IV) often require a short period of saturation-free time [5]. This makes the time to saturate a useful metric when sizing the CT.

$$T_S = -\tau \cdot \ln \left( 1 - \frac{(K_S - 1)}{\left( \frac{X}{R} \right)} \right) \quad (6)$$

## C. IEC Guidance

If system data are available,  $K_S$  can be calculated using (5), which can then be used to obtain the time to saturate ( $T_S$ ) by using (6). But, if we start with  $T_S$ , we can rearrange (6) to solve for  $K_S$ , as shown in (7) and Fig. 3. Neither  $T_S$  from (6) nor  $K_S$  from (7) consider the effect of  $\theta$ . However, they serve as the basis of the guidance provided by IEC [2].

$$K_S = 1 + \omega_n \cdot \tau \cdot \left( 1 - e^{-\frac{T_S}{\tau}} \right) \quad (7)$$

Saturation occurs when the magnetizing branch voltage ( $V_M$ ) exceeds the saturation voltage ( $V_{SAT}$ ) and can be evaluated by varying  $\theta$  in (3). When obtained analytically considering the effect of  $\theta$ ,  $K_S$  becomes the transient factor  $K_{TF}$ . Like  $K_S$ ,  $K_{TF}$  corresponds to the ratio by which the CT is sized relative to a purely symmetrical fault current and can be evaluated via (5).

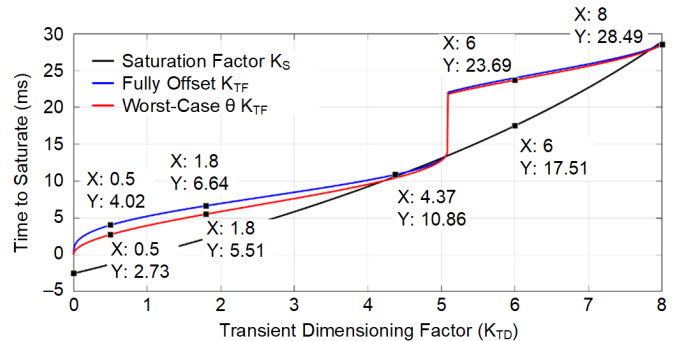


Fig. 3. Time to Saturate Versus CT Transient Dimensioning Factor for a 60 Hz System With  $\tau = 30$  ms

In Fig. 3, the blue trace represents the  $K_{TF}$  for the fully offset flux waveform shown in Fig. 2b. However, for small values of  $T_s$ , other fault inception angles have a steeper current rise than the fully offset current shown in Fig. 2a. This results in a greater development of  $\phi_M$ , as evident in Fig. 2b, which then translates to a higher  $K_{TF}$ , as shown via the red trace in Fig. 3. The discontinuities in the blue and red traces are due to the increasingly offset, sinusoidal flux not accumulating unidirectionally at every instant in time, as depicted in Fig. 2.

As is evident from Fig. 2 and Fig. 3,  $K_{TF}$  is a function of the fault inception angle, time, and system X/R ratio. When the worst-case  $K_{TF}$  is determined via analysis, simulations, and test methods like those described later in this paper, it becomes the transient dimensioning factor,  $K_{TD}$ .  $K_{TD}$  is a constant that can be used to size a CT by substituting  $K_{TD}$  for  $K_S$  in (5). It is ideally provided by the relay manufacturer for a given application and device [2].

#### D. Effect of X/R Ratio

As explained previously, if the CT is over-dimensioned to carry  $(1 + X/R)$  per-unit flux in the linear region, it will not saturate irrespective of the fault inception angle, assuming there is no remanence. This criterion to avoid saturation is represented in physical quantities by (8) from IEEE [1].

$$V_{SAT} > \left(1 + \frac{X}{R}\right) \cdot \left(\frac{I_p}{N}\right) \cdot (R_{CT} + R_B) \quad (8)$$

Protection elements that are vulnerable to degraded performance due to CT saturation are often designed to tolerate some saturation. For such cases, application guidance has been provided in the past where a fraction of the value obtained via (8) can be used to size CTs [6] [7].

Due to the large X/R ratios near generating plants, typical CTs do not quickly or deeply saturate but rather do so only after some time due to the long-lasting decaying dc. For such high-X/R systems, applying (8) and linearly scaling it with a fraction can still make sizing CTs very challenging.

However, by using (7) to consider the CT sizing we expect the CT requirements to scale exponentially instead of linearly with respect to the X/R ratio, as shown in Fig. 4 for four values of  $T_s$ .

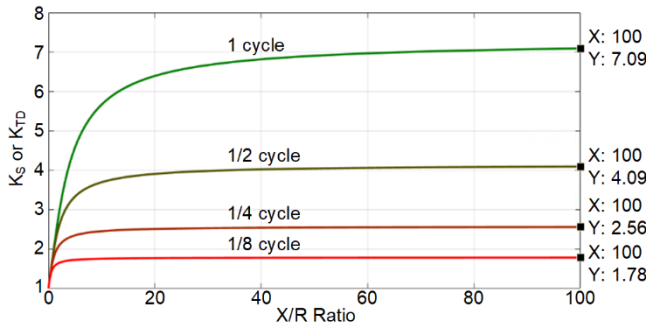


Fig. 4. CT Dimensioning Factor Based On System X/R Ratio

As we get to larger X/R ratios, the CT dimensions represented on the y-axis do not need to increase significantly. This is consistent with (9) from IEC, where the X/R ratio, while

a factor, is not a critical parameter for CT sizing.  $E_{AL}$  in (9) is the emf at the accuracy limit used by IEC, analogous to the  $V_{SAT}$  value used for ANSI CTs, and is also defined at the CT magnetizing branch.

$$E_{AL} > K_{TD} \cdot \left(\frac{I_p}{N}\right) \cdot (R_{CT} + R_B) \quad (9)$$

#### E. Voltage Rating and IEEE CT Class

Until now, most of the discussion has been confined to the magnetizing branch voltage and is true when considering time-to-saturate equations [1] or transient factors [2]. The most commonly applied ANSI CT for protection applications is the Class C CT, where the ANSI voltage ratings ( $V_{ANSI}$ ) are defined at the secondary terminals of the CT [1]. Defining the ANSI voltage rating at the CT terminal plays a role in generating plants where CT ratios (and consequently  $R_{CT}$ ) can be large, making the difference between  $V_M$  and  $V_B$  glaringly significant. For instance, a C200 10000:5 CT may have a saturation voltage higher than 700 V at the magnetizing branch; hence, it is likely physically bigger than a lower ratio C200 CT. This is not the case when sizing an IEC CT, where the sizing is done using  $E_{AL}$ , which is calculated at the magnetizing branch, as shown by accounting for  $R_{CT}$  in (9).

#### F. Remanence and IEC CT Classes

Until now, our discussion has assumed no remanence. But, CTs can have a significant level of remanence. When a fault current is interrupted near a current zero-crossing, the flux density in the core can be large, such as at Points A or B of the B-H curve shown in Fig. 5.

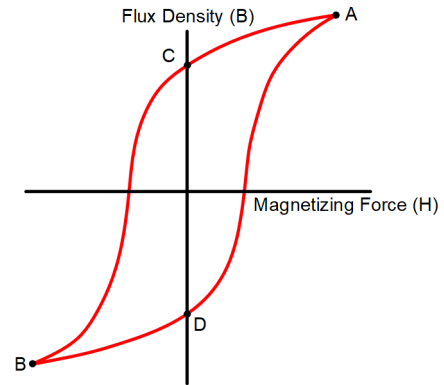


Fig. 5. Typical B-H Curve of a Non-Gapped CT

Following interruption of the primary current, the energy stored in the magnetic field of the core must dissipate through the CT secondary circuit ( $R_B + R_{CT}$ ), as shown in Fig. 6.

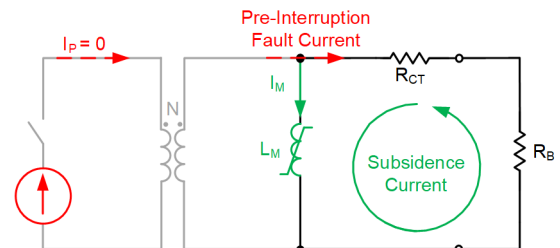


Fig. 6. Effect of Subsidence Current on Remanence (Circuit)

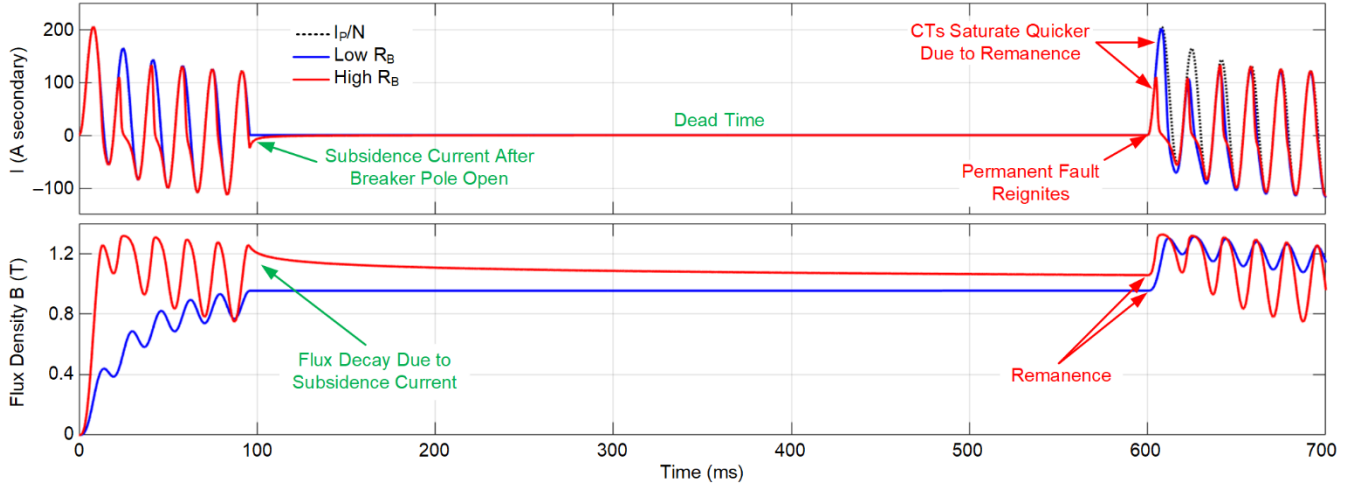


Fig. 7. Effect of Subsidence Current on Remanence Over Time

This results in a subsidence current that decays as the magnetic energy in the core is released, thus lowering remanence during the autoreclose dead time (as shown in Fig. 7). At this point, the flux density moves to Points C or D from Points A or B in Fig. 5, with the CT left partially magnetized with remanence in its core.

When load current is reapplied, there is a further reduction in remanence, which depends on the initial value of the residual flux, the ac flux produced by the load current, and the characteristics of the CT core [8]. Fig. 8 shows test results for one type of CT core material. We notice that the level of flux densities that are required to demagnetize a protection-class CT substantially (with a large dynamic range) are not expected from load currents [8]. However, the slopes of the curves of Fig. 8 are steepest near the y-axis, indicating that load current will indeed lower remanence, even if by a small amount. Load currents in a generating plant are also typically a larger percentage of the fault current compared to some other applications, which may provide a favorable, lower remanence.

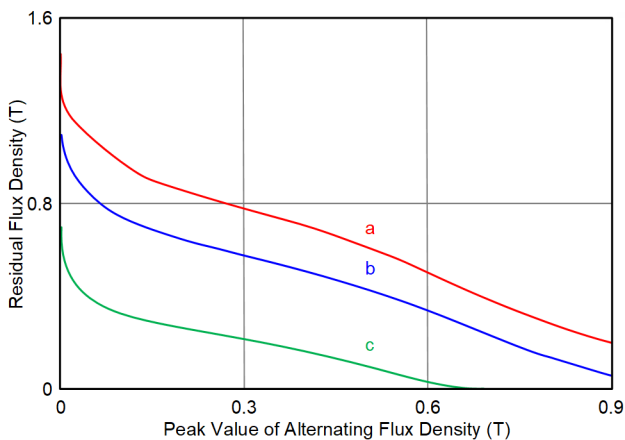


Fig. 8. Effect of Applied Steady-State Flux on Remanence [8]

An old survey of 141 CTs on a 230 kV system shared in the 1996 revision of IEEE C37.110 indicates that the upper range of remanence in the CTs was 61 to 80 percent [1]. This is consistent with the survey done by IEC [2], the results of which are shared in Table I. CTs prior to the 1990s were made of materials that held a maximum remanence of 77 percent. CTs

that have been manufactured since the 1990s have newer core material that can hold more remanence [2].

TABLE I  
THEORETICAL AND MEASURED REMANENCE FACTORS [2]

	Old CT Cores (1930 to 1990)	New CT Cores (since 1995)
<b>Maximum Remanence<sup>a</sup></b>	75% to 77%	88% to 95%
<b>Actual Remanence<sup>b</sup></b>	70% to 75%	85% to 87%

<sup>a</sup>Maximum possible remanence limited by the hysteresis curve

<sup>b</sup>Actual residual remanence measured after de-energization, commissioning, or other tests

For CTs in generating plants, external system faults, poor synchronization events [9], or other causes can result in remanence [2]. This makes the level of remanence (Rem) unpredictable, and the guidance from (9) would have to be multiplied by a remanence dimensioning factor ( $K_{REM}$ ) provided by (10) [1] [2]. For instance, for an older CT with 80 percent maximum remanence ( $Rem = 80\%$ ),  $K_{REM}$  would be 5.  $K_{REM}$  is then multiplied by (9) to obtain (11).

$$K_{REM} = \frac{1}{1 - Rem} \quad (10)$$

$$E_{AL} = K_{REM} \cdot K_{TD} \cdot \frac{I_p}{N} \cdot (R_{CT} + R_B) \quad (11)$$

As noted earlier, newer CTs can hold substantially higher remanence—up to 95 percent. This corresponds to a  $K_{REM}$  of 20 and very large CTs. IEC provides the alternative CT classes shown in Table II as countermeasures to remanence. Non-gapped CT classes, such as P, PX, and TPX, that may normally store high remanence can be introduced with a tiny gap (e.g., 0.1 percent of circumference) to gain anti-remanence properties ( $Rem < 10\%$ ). These CTs can then be classified as PR, PXR, and TPY, respectively. The effects of gaps on remanence can be seen in Fig. 9 [10]. When a fault is cleared, the decay in remanence during the dead time (Fig. 7) causes the flux to move from a high value to  $B_r(1)$  for a non-gapped CT. In the case of a gapped CT, however, the flux instead moves to a much lower value  $B_r(2)$ .

TABLE II  
EFFECT OF GAPPED AND NON-GAPPED CORES [2]

	Remanence	Anti-Remanence	High DC Damping
P, PX, TPX	X		
PR, PXR, TPY		X	
TPZ		X	X

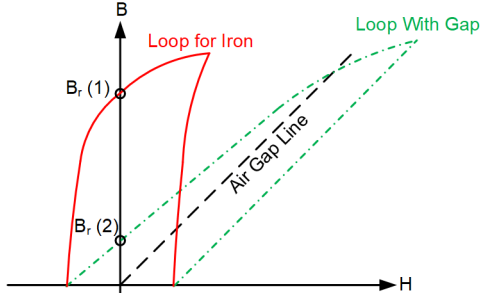


Fig. 9. Effect of Air Gap on Remanence [10]

Gaps reduce the slope of a CT's linear operating region, as shown in Fig. 10.

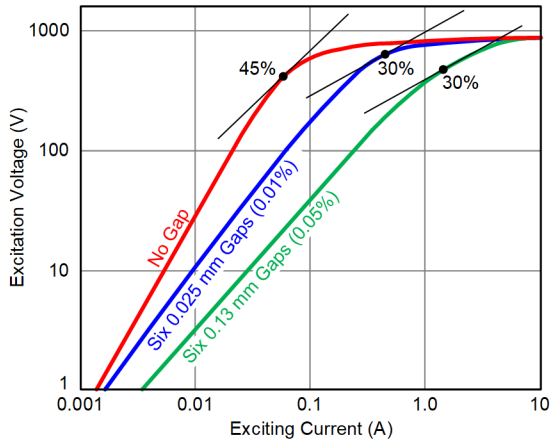


Fig. 10. Effect of Air Gap on Excitation Curve [10]

TPZ CTs have relatively large gaps and a significantly lower slope in their excitation characteristics, corresponding to a lower relative permeability ( $\mu_r$ ) and associated magnetizing inductance ( $L_M$ ). This results in a substantially lower secondary network time constant ( $< 0.1$  s) than for the other anti-remanence classes ( $> 1$  s) or for non-gapped CTs ( $\sim 10$  s) when the CT operates in the linear region. A lower secondary network time constant results in the “high dc damping” referred to in Table II, making the CT not very capable of reproducing dc from a fault current or an inrush. This can penalize some protection element designs (as discussed in Section IV, Subsection B) and is an application consideration when selecting CTs.

A reduced slope in a CT's excitation characteristic (Fig. 10) also translates to a greater magnetizing current and standing error in the linear operating region. Over time, better materials with higher  $\mu_r$  have been used for CT manufacturing, hence increasing the slope of the linear region and resulting in lower losses, less steady-state magnetizing current, and greater accuracy.

This benefits metering applications, but protection applications generally do not need such level of accuracy; they need better transient performance. A sharp rise in the linear region in some CT designs leads to a sharp saturation region, which makes the knee voltage ( $V_{KNEE}$ ) a larger percentage of the saturation voltage ( $V_{SAT}$ ). Note that while  $V_{KNEE}$  has been defined differently by IEEE [1] and IEC [2], they both intend to describe the onset of saturation for a CT. We know that CTs cannot remain saturated for a long time while carrying load current. If they did, the magnetizing branch would draw significant current, which would counteract the flux buildup, similar to the effect shown in Fig. 7. We also know that a significant magnetizing current is drawn at  $V_{KNEE}$ , whereas the CT is sized according to  $V_{SAT}$ . This information is available in the CT data sheet and can be obtained via inspection. For non-gapped IEC protection CTs, we assume a maximum remanence level of 80 percent ( $K_{REM} = 5$ ). For ANSI CTs, we assume a maximum remanence level of 67 percent ( $K_{REM} = 3$ ), which provides adequate margin compared to prior references that indicate a level closer to 50 percent [11].

Other considerations on the impact of remanence include the fact that a fault will not always have the worst possible magnitude or inception angle for a given application. CTs are also often reasonably well matched and may hold a similar level of remanence for a through fault. Fifty percent of the time remanence is expected to be in opposition to the flux resulting from the fault current. As indicated earlier, during an autoreclose, remanence can be large, but during this time many algorithms (such as the one discussed in Section IV, Subsection A) may still exhibit enhanced security and avoid having an issue. Finally, as explained previously, if remanence is left in the core after resuming steady-state operation, load current is expected to reduce remanence a little bit and prepare the CT for the next through fault.

Generally, fast protection elements that are expected to operate at subsample speeds and are susceptible to CT saturation must consider remanence. However, in Section IV we show how modern relays with careful protection element design supported by simple application guidance can alleviate such concerns. This allows application of non-gapped CTs, such as the ANSI C classes and the IEC P/PX/TPX classes, as is shown via practical examples in the appendix. If CT dimensioning is still a challenge, then the anti-remanence classes from Table II may be applied.

#### G. Other Considerations

In addition to factors discussed already, other factors affect relay performance, such as the protection scheme, application settings, factory parameters, and relay hardware. Generator differential relays protecting black-start units may also have to consider external transformer inrush. Relays typically also have an internal CT that adds to the saturation from the primary CT. The effect is lower, since saturation of the primary CT reduces the current seen by the relay's internal CT. Considering the numerous factors that affect relay performance, guidance for CT application is relay-dependent and is best provided by the relay manufacturer based on tests [2].

### III. CT MODELS

In the past, the use of CT models was promoted for CT selection, analysis, and the development of relay settings. But, modern relays have advanced algorithms that make it difficult to simply use these models and apply the results. For this reason, it becomes the manufacturer's responsibility to test the relay and provide adequate CT requirements and setting guidelines [2], which is the focus of this paper. To develop such application guidance, we needed to understand the CT equivalent circuit of Fig. 1 in more detail than explained in Section II. This allowed us to create accurate digital models, perform tests, and determine CT requirements.

Various tools have been used to model CTs [3] [12] [13] [14]. The models can be classified as follows by the approach they use to model the non-linear magnetizing inductance ( $L_M$ ):

1. Using physical CT parameters and representing the non-linearity of the magnetizing branch by using the S-shaped Frolich equation [12] [13].
2. Using CT excitation curve data [3] [13] [14] typically available from data sheets or via testing [15].

Both classes of models require the basic circuit parameters from Fig. 1 that are linear, such as  $N$ ,  $R_{CT}$ ,  $L_{CT}$ ,  $R_B$ , and  $L_B$ . All models allow an initial remanence value ( $B_0$ ) to be provided.

#### A. Physical CT Model Using Frolich Equation

The physical CT model requires information such as the maximum relative permeability of the core material ( $\mu_r$ ), core path-length ( $L$ ), maximum magnetic flux density ( $B_{MAX}$ ), and the saturation voltage of the CT ( $V_{SAT}$ ), which is typically defined at the magnetizing branch. Subsequently, the Frolich model [12] using a typical  $B_{MAX}$  of 1.5T is used to generate the S-shaped saturation characteristic shown in Fig. 11. Having to enter the physical parameters of the Frolich equation may appear to be a disadvantage if those data are not available.

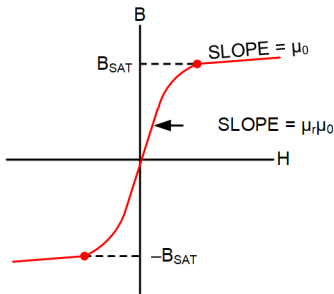


Fig. 11. S-Shaped Hysteresis Curve Using Frolich Equation

Using a C400 CT, we varied  $\mu_r$  from 5000 to 10000 and  $L$  from 1 m to 2 m. The results are shown in Fig. 12, which shows that the physical model is not extremely sensitive to the magnetic parameter errors as long as the saturation voltage is accurate.

Gapped CTs can be modeled by lowering  $\mu_r$ , hence decreasing the curvature of the S-shape. The Frolich equation does not model the hysteresis described in Fig. 5 [12]. Despite these minor limitations, it has been used to provide guidance for protective relaying applications [6] [16].

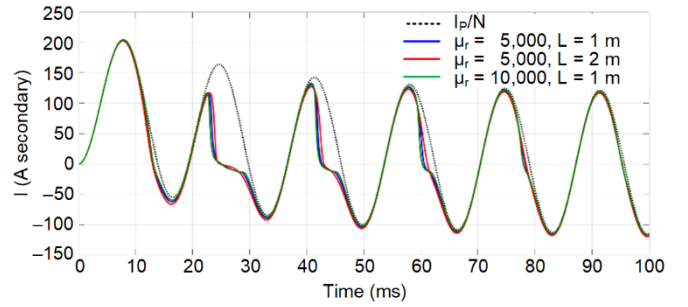


Fig. 12. Parameter Sensitivity for a C400 Physical Model

#### B. Excitation Curve-Based CT Model

CT models based on an excitation curve use data available from data sheets or via testing [15]. One such test was done using a small C10 CT, as shown in Fig. 13 [17]. Varying voltage levels were applied to the CT secondary ( $V_B$  in Fig. 1) with the CT primary left open. The measured current corresponds to the CT magnetizing current ( $I_M$ ), which, when compensated for the CT internal resistance ( $R_{CT}$ ), allowed determination of the excitation curve of Fig. 13.

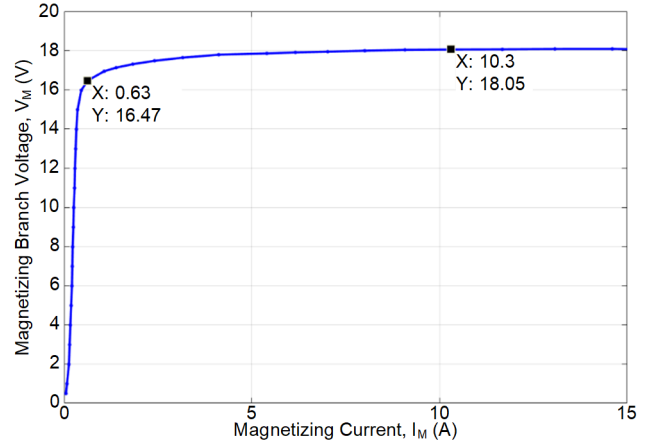


Fig. 13. Excitation Characteristic of a C10 CT Obtained Via 60 Hz Test [17]

Some models only require  $V_{SAT}$  and model the saturation region with a slope ( $S$ ) [3]. Fig. 14 shows the performance of an excitation curve-based model at different slopes [3]. Again, the response of the model for a different value of  $S$  is not very different and is well within typical engineering margins. The accuracy of the excitation curve is not as critical as long as the saturation voltage is accurate. Comparing Fig. 12 and Fig. 14 shows that the physical model and the excitation model exhibit similar performance.

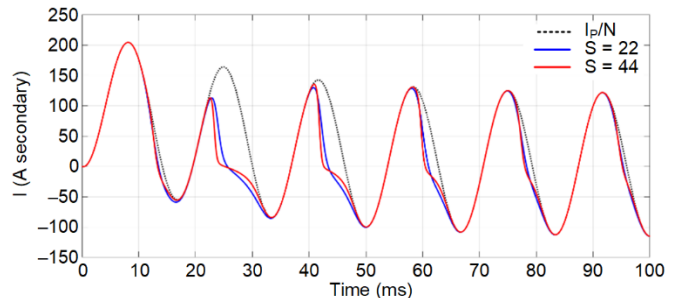


Fig. 14. Parameter Sensitivity for a C400 Excitation Curve Model

Other excitation models use more CT data and can model behavior such as remanence and subsidence more accurately, as shown in the example of Fig. 7 [13] [14].

### C. Model Validation

We validated the CT models of [3] and [12] with lab test data from an ANSI C10 150:5 CT where  $R_{CT} = 51 \text{ m}\Omega$  and  $R_B = 36 \text{ m}\Omega$  [17]. A fully offset rms current of 1,420 A primary (47.3 A secondary) with an X/R ratio of 11.31 and  $\theta = -85^\circ$  was applied to the CT. The parameters that affect the magnetizing branch are shown in Table III.

TABLE III  
MAGNETIZING BRANCH PARAMETERS USED FOR CT MODELS

Parameter	Data
$\mu_r$ (physical model)	5000
L (physical model)	0.10 m
$B_{MAX}$ (physical model)	1.5 T
S (excitation model)	15 A/V
$V_{SAT}$ (both models)	18 V
Remanence (both models)	0 pu

Fig. 15 shows that both models perform reasonably well in relation to the real lab CT.

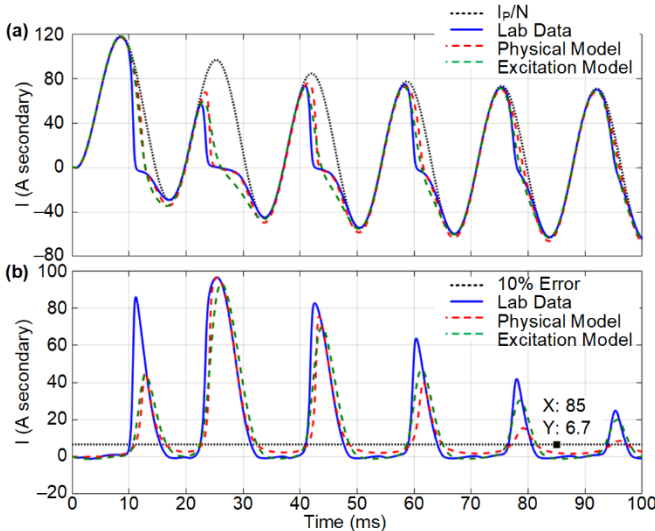


Fig. 15. Comparison of Laboratory Data and Models Using Secondary Currents (a) and Excitation Current (b)

The lab CT saturates first at 10.13 ms, the excitation CT model at 10.75 ms, and the physical CT model at 11.13 ms. The time to saturate is based on the definition in [1], where the error due to CT magnetizing current is 10 percent.

We confirmed that the CT models are all reasonably accurate by using the time-to-saturate equations of Fig. 3 for a fully offset waveform. Using (5) with a  $V_{SAT}$  of 18 V,  $I_S$  of 47.3 A rms, and an  $R_{CT} + R_B$  of 87 m $\Omega$ , we calculated a  $K_{TD}$  of 4.37. Considering Fig. 3, this corresponds to a time to saturate of 10.86 ms, in the range of what we obtained from the real CT and the two models and consistent with the model used in [17].

### D. Summary

The models of [3] and [12] are not extremely sensitive to magnetic parameter errors other than the saturation voltage, making them reasonable for use in determining CT requirements as discussed in Section V. We validated the simplified models of [3] and [12] using a real CT in the laboratory. Testing with a real CT is not always an option for validating a model. An alternate approach may be to compare the time to saturate from the model to the expected time to saturate based on (1), (2), and (3) in Section II and represented in Fig. 3. Note that using (6), as shown in Fig. 3, may produce larger errors and lead to oversizing.

## IV. PROTECTIVE RELAY ALGORITHM

Most modern differential relays provide enhanced security if there is a possibility of CT saturation [5]; otherwise they continue to use sensitive characteristics. A simplified version of the modern differential algorithm considered in this paper is shown in Fig. 16.

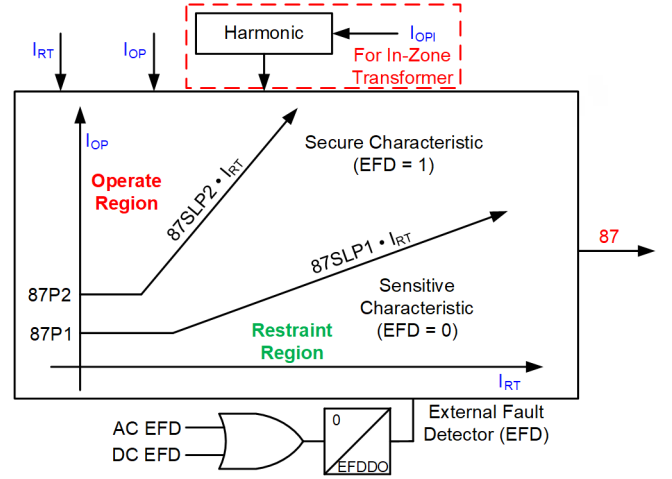


Fig. 16. Characteristic of a Differential Relay Zone

There are a couple of advantages to an adaptive scheme like the one shown in Fig. 16:

1. There are no additional user settings and the transition  $I_{RT}$  level from 87SLP1 to 87SLP2 does not need to be calculated, unlike in older dual-slope designs.
2. Some relays that use a fixed dual-slope characteristic may lose security for high-current external faults when CTs saturate, which lowers the available restraint and potentially encroaches on the sensitive characteristic.

The differential scheme in consideration has two zones and runs every 2.5 ms.  $I_{OP}$  is the operating current and is defined as the phasor sum of all the currents in the zone.  $I_{OPI}$  is raw operating current derived from the current samples.  $I_{RT}$  is the sum of the current magnitudes comprising the zone.  $I_{RTI}$  is the raw restraint derived from the current samples.

A typical application would be to set the first zone to protect the generator and the second zone to protect the transformer. The parts of the scheme applicable to this paper are discussed in this section.

### A. AC External Fault Detector

When an external fault occurs, the restraint current ( $I_{RT}$ ) current seen by a differential relay is expected to suddenly increase, whereas the operate current ( $I_{OP}$ ) should not. The scheme uses this principle and expects CT saturation to not occur immediately.

If the change in  $I_{RT}$  is larger than 1.25 pu of the rated current of the generator or the transformer winding while the operate current does not see half the change for some time, the ac EFD asserts (Fig. 17). Since this change is designed to only be detected at fault inception, the dropout timer EFDDO in Fig. 16 must be set greater than any autoreclose time delays (e.g., 1 s). This alleviates concerns regarding a large remanence during an autoreclose sequence where a permanent fault could induce fast and deep CT saturation (Fig. 7).

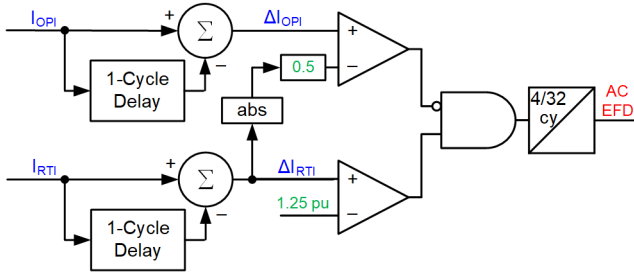


Fig. 17. AC EFD Logic

Various algorithm design choices, such as the following, affect CT sizing requirements:

- Using instantaneous operate ( $I_{OP}$ ) and restraint current ( $I_{RT}$ ) may favor CT requirements compared to algorithms that use phasors [5].
- Factory constants (e.g., 0.5, 1.25 pu and 4/32 cycles).
- The definition of restraint current, which can differ between relay designs [18].

Determining CT requirements for a given scheme via testing, as discussed in Section V, may be the only reliable way to evaluate scheme performance and provide application guidance.

### B. DC Saturation

As discussed in Section II, dc offset in currents may cause CTs to saturate. This is the principle used by modern generator differential relays to add security to the differential scheme [5]. If the level of dc in the currents comprising the zone is determined to be sufficiently large (via use of a 1-cycle average calculation) for 50 ms, the dc EFD picks up via the logic of Fig. 18. The logic checks that there is a low level of differential current ( $I_{OP} < 50$  percent of  $I_{RT}$ ) to not desensitize the differential element for an internal fault. The dc EFD secures the relay before the CT saturates and is a preventative algorithm, just like the ac EFD of Fig. 17.

The dc EFD is especially beneficial to an 87G element for black-start applications, particularly where there is a low-side breaker and the generator is required to energize the generator step-up unit (GSU) transformer. Transformer inrush for the 87G element is an external condition and has no primary system contribution to the operate current. However, if the transformer

energization is unipolar in nature, as is often the case in two phases, then it also contains a large amount of dc.

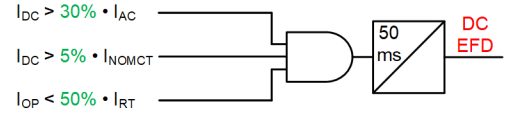


Fig. 18. DC EFD Logic

Over time, the unipolar current builds unidirectional flux in the CTs, resulting in saturation. Even if the CTs respond well, the relay internal CTs may saturate, as shown in Fig. 19. Unequal saturation of the CTs, internal or otherwise, comprising the 87G zone may result in a misoperation.

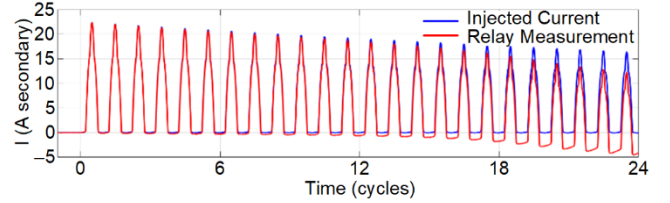


Fig. 19. Relay Internal CT Response for a Unipolar Inrush

### C. Harmonic Detector

The current during transformer inrush enters the 87T zone but does not leave, behaving as an internal fault and resulting in a non-zero  $I_{OP}$ . However,  $I_{OP}$  typically has harmonics and is the principle used to secure an 87T element during an inrush. Harmonic detectors are not designed to detect CT saturation; hence, they are not within the scope of this paper. But, they may inadvertently add security while trading element operating speed for 87T applications [19].

Harmonic detectors are not applied to the 87G element since any inrush condition corresponds to a through current ( $I_{RT}$ ), and if the CTs perform well, the result would be zero differential current ( $I_{OP}$ ).

## V. CT REQUIREMENTS FOR 87G AND 87T ELEMENTS

Using the CT model from Section III, we evaluated the performance of the relay algorithm described in Section IV. The most conservative guidance for differential applications is to assume that one CT saturates to a degree and the other does not. It is important to test this way since the magnetizing characteristic of a CT is non-linear and even a small mismatch in burden impedance due to the lead length can manifest in a large difference in transient CT performance. Other considerations include the use of CTs from different manufacturers or different models from the same manufacturer installed as part of separate projects [20]. This could occur in a generating station, for example, where the generator neutral-side CTs may be owned by the generator owner and the terminal CTs may be owned by the switchgear manufacturer.

Another testing consideration, as is apparent from Fig. 19, is that the internal CT of a relay can also saturate. As such, it is important to demagnetize the CT after each hardware-in-the-loop simulation. As supported by the results from [8], a large ac flux can reduce CT remanence (see Fig. 8). A large ac flux can be produced by injecting a low-frequency current (e.g.,

3 Hz) with a large current magnitude (e.g., 5 times nominal) followed by a negative current magnitude ramp to leave the CT demagnetized. The maximum current should respect the relay's thermal ratings (e.g., 1 minute at 5 times nominal) followed by a long enough cooldown time. Despite choosing a signal with such a large effective flux (100 times nominal), the demagnetization process can take minutes.

To develop the CT requirements and setting criteria for the differential element provided in this section, we found it quicker and simpler to model the internal CT of the relay and to then use it to test the relay algorithm [12]. Modeling allows a bulk of the testing to be done with simulated signals, avoiding tests with large currents and long demagnetization times. To ensure the accuracy of the results, we spot-checked the resulting guidance by executing hardware-in-the-loop tests and demagnetizing the CT [13].

#### A. CT Ratio

The CT ratio should be selected such that the rated current (including a 50 percent margin) does not exceed the CT nominal rating [1]. The maximum symmetrical through fault current seen by the CT should not exceed 20 times the nominal CT rating [1], which is generally not a concern for the applications considered in this paper. This is a design criterion often used by relays to define the dynamic current range, beyond which electronic components such as analog-to-digital converters saturate. Choosing a higher CT ratio can also allow the selection of a CT with a lower voltage rating [20].

#### B. 87G and 87T CT Sizing and Settings

To obtain the CT sizing and setting guidance in this subsection, we used a power system model to apply external faults to the algorithms described in Section IV. The details of the tests are as follows:

- The point-on-wave of fault inception for the external fault was varied from 0 to 360 degrees.
- The system X/R ratio was varied up to 100.
- Both ground and phase faults were applied.
- One CT was considered ideal with the scaled secondary current applied to the zone. The other CT comprising the differential zone was saturated with varying  $R_B$  to emulate different CT dimensioning factors.
- 87P1 was set to 0.10 pu, and 87SLP1 was set to 10 percent. These sensitive settings minimized possible interference with the test.
- The current from the saturated CT was scaled by a factor of 0.95 to add 5 percent overall margin to the test.
- For each CT size, the 87SLP2 settings were varied from 10 to 90 percent to check the value at which the differential element misoperated.

The CT sizing requirements and corresponding 87SLP2 settings obtained via this procedure are shown in Fig. 20. Without considering remanence, the minimum CT size that allows this scheme to be applied corresponds to a  $K_{TD}$  of 1.8. Fig. 20 shows that, instead of having to over-dimension the CT

by a factor greater than 50 ( $1 + X/R$ ) near a generating plant to account for the decaying dc [1], a factor less than 2 will suffice.

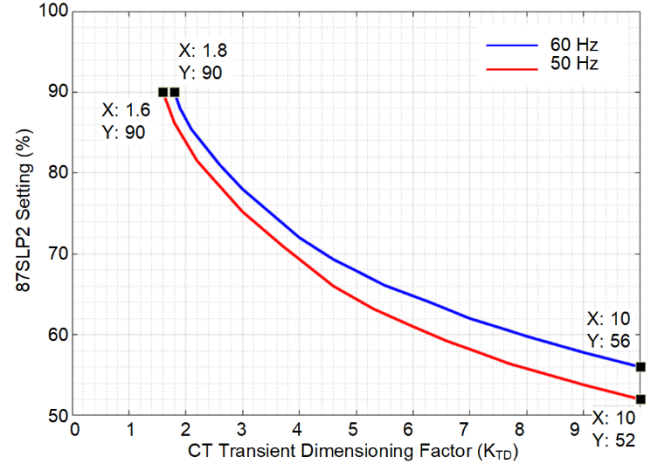


Fig. 20. Application Guidance for the Differential Element Without Remanence

In keeping with the IEC definitions [2] the overall selection criteria for sizing a CT is defined as shown in (12).

$$E_{AL} = (K_{REM} \cdot K_{TD}) \cdot \left(\frac{I_F}{N}\right) \cdot (R_B + R_{CT}) \quad (12)$$

Per ANSI convention (Section II, Subsection E), the rated voltage ( $V_{ANSI}$ ) is defined at the secondary terminals. The CT manufacturer accounts for the CT internal voltage drop to ensure less than 10 percent error up to a value of 20 times the nominal CT current [1]. When considering protective relays, the 20-times-nominal factor originates from  $K_S$  (saturation factor),  $K_{REM}$  (remanence dimensioning factor),  $I_F$  (primary fault current), and  $N$  (CT ratio). For our generating system application, these values would be 1.8 (Fig. 20), 3 (Section II, Subsection F), 5 pu (generating station), and 1.5 (Section V, Subsection A), respectively, which when accounted for are approximately 20, when considering (13). A value less than 20 translates to conservative guidance, allowing (13) to be used as an initial estimate for CT sizing.

$$V_{ANSI} > (K_{REM} \cdot K_S) \cdot \left(\frac{I_F}{N}\right) \cdot (R_B) \quad (13)$$

If  $R_{CT}$  is available from a CT data sheet [16], the calculation of (14) may be performed. However, comparing  $V_{SAT}$  in (14) to the C-rating voltage ( $V_{ANSI}$ ) can be excessively conservative when  $R_{CT}$  is large. A large  $R_{CT}$  is typical of high-ratio CTs and makes the difference between the magnetizing and burden voltages substantial.

$$V_{SAT} = (K_{REM} \cdot K_S) \cdot \left(\frac{I_F}{N}\right) \cdot (R_B + R_{CT}) \quad (14)$$

A better comparison accounts for the voltage drop already considered by the CT manufacturer via (15), where  $I_{NOM}$  is the CT nominal current (e.g., 5 A). The value provided by (15) is conservative since ANSI rounds down the voltage rating.

$$V_{SAT\_CT} = V_{ANSI} + 20 \cdot I_{NOM} \cdot R_{CT} \quad (15)$$

If available, the most accurate comparison is to refer to the CT excitation curve to obtain the saturation voltage of the CT where the excitation current is 10 A (twice  $I_{\text{NOM}}$ ).

Regardless of the application, an ANSI CT smaller than C100 or an IEC CT with an accuracy limit factor (ALF) smaller than 20 should not be used when applying the scheme discussed in Section IV. ALF is the ratio of symmetrical current with respect to CT rated current for which the manufacturer guarantees that the CT meets the error criteria (e.g., 5 percent for a 5P IEC CT) when the rated burden is connected. For an ANSI CT, ALF is 20 since the manufacturer guarantees a 10 percent accuracy at 20 times the symmetrical fault current. Furthermore, a minimum VA rating of 2.5 for 1 A CTs and 25 for 5 A nominal CTs should be selected. CTs lower than a C100 rating are generally associated with B ratings (e.g., B-0.5) [1] and not with the standard C ratings used with protective relays. The VA rating of 25 with an ALF of 20 for an IEC CT is equivalent to a 5 A nominal C100 ANSI CT. The appendix shows how the above guidance is used for a sample application.

The 87SLP1 setting in the differential scheme of Fig. 16 addresses inaccuracies resulting from steady-state operation or slow transients not associated with CT saturation. For the 87G element, these inaccuracies result from relay measurement or CT errors and require an 87SLP1 setting larger than 10 percent. For the 87T element, the 87SLP1 setting must additionally account for the tap changer, if applicable [18].

### C. 87G Application Guidance for Black-Start Units

For black-start applications where the generator is required to magnetize the GSU transformer, the 87G element may see inrush through current which, due to unequal CT performance (Fig. 19), may result in a misoperation. To obtain the application guidance in this subsection, a transformer was energized with a low-side breaker to obtain a large inrush current. The same general process outlined in Section V, Subsection B was used. The only significant differences are as follows:

- Given that the CT over-dimensioning is not well defined for an inrush current, the maximum external fault current for the 87G element was used to dimension the CT. A minimum dimensioning factor of 1 was tested.
- The inrush current was scaled down to find the value where the ac EFD (Fig. 17) deasserts. This is the upper limit, above which we considered the algorithm secure due to 87SLP2.
- At the upper limit, the minimum pickup for the secure characteristic (87P2) was varied to find the value at which the differential scheme misoperated.
- The inrush current was scaled down to find the value where the dc EFD deasserts (Fig. 18). This is the lower limit.
- At the lower limit, 87P1 was varied (with 87P2 set to 87P1) to check the value at which the differential scheme misoperated.

The results from the tests are summarized as follows:

- If the inrush current is high, the ac EFD (Fig. 17) picks up and secures the differential scheme.
- For moderate inrush, where the ac EFD (Fig. 17) remains deasserted and the dc EFD is asserted (Fig. 18), 87P2 secures the differential scheme. Significantly smaller values than what is shown in (16) may result in misoperations for moderate inrush conditions due to unequal CT performance.

$$87P2 = 0.50 \text{ pu} \quad (16)$$

- If the inrush current is low when the transformer is energized, the pickup of the sensitive element provides security. This is the case where neither EFD (Fig. 17 or Fig. 18) picks up. Since the dc EFD threshold is defined in secondary amperes and  $I_{\text{OP}}$  is defined in per-unit, 87P1 is set according to (17), where  $I_{\text{NOM}}$  is the rated secondary current of the CT (e.g., 5 A) and TAP is the rated secondary current of the generator (e.g., 3 A).

$$87P1 = 0.15 \cdot \left( \frac{I_{\text{NOM}}}{\text{TAP}} \right) \text{ pu} \quad (17)$$

As explained in Section II, Subsection F, TPZ CTs provide high DC damping, which interferes with the dc EFD logic shown in Fig. 18. It is best not to apply TPZ CTs if any of the other CT classes can be used. If, however, TPZ CTs are already applied, then 87P1 should be increased to the value of 87P2.

### D. Summary

In this section we looked at test methods, application considerations, CT sizing requirements, and setting guidance for a generator and transformer differential scheme. A smaller  $K_{\text{TD}}$  corresponds to a smaller CT and indicates an algorithm with more relaxed CT requirements. An ac EFD that works on raw samples ( $I_{\text{OP}}$  and  $I_{\text{RT}}$  in Fig. 17) is likely to reduce the  $K_{\text{TD}}$  requirement compared to older phasor-based detectors [5]. Similarly, if the differential scheme does not have a dc EFD (Fig. 18), the settings may need to be more secure.

Redrawing Fig. 3 (as shown in Fig. 21) for a system near a generating plant with a much higher X/R ratio of 60, shows that a  $K_{\text{TD}}$  of 1.8 effectively translates to a  $T_{\text{s}}$  of  $\sim 5.3$  ms, which is larger than the pickup timer for the ac EFD of 2.5 ms. The difference is related to the physical relay hardware, added margin during testing, and relay design factors, such as algorithm execution rate, security counts, the equation used to calculate  $I_{\text{RT}}$ , and factory constants such as the  $\Delta I_{\text{RT}}$  threshold in Fig. 17.

An application example for the guidance provided in this section is provided in the appendix, where ANSI and IEC CTs are sized for an 87G and 87T application.

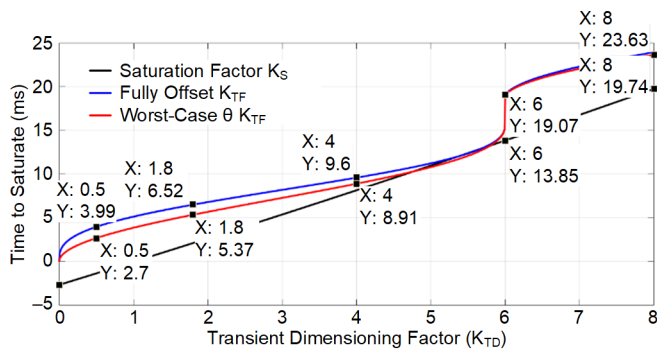


Fig. 21. Time to Saturate Versus CT Transient Dimensioning Factor for a 60 Hz System With High X/R = 60

Note that the guidance provided in this section assumes that the full ratio of the CT is used. If a multi-ratio CT is used and tapped at a different value, the appropriate derating must be performed according to standard practices [1] [2].

## VI. CONCLUSION

Security is the paramount property of a protective relay. Relay elements that are susceptible to CT saturation should have simple and easy-to-use application guidance, allowing a clear definition of the security limit for the element. Once the security limit is defined, other performance metrics, such as sensitivity and speed, may be evaluated for a given scheme and application settings.

We looked at the similarities and differences between the guidance provided by IEEE and IEC. Both guides provide similar mechanisms to account for the dc transient during a fault and remanence. Other factors, such as the relay algorithm and hardware, also affect CT requirements.

Using CT models that were validated with a physical CT, along with hardware-in-the-loop testing, we determined the CT requirements for a generator and transformer differential scheme in a relay. We show that modern relays use algorithms that can drastically reduce CT requirements. Finally, we use the application guidance to size both ANSI and IEC CTs and obtain relay settings for a generator and transformer differential relay for an example generating plant.

## VII. APPENDIX

### A. System Data

In this section, we demonstrate the use of the application guidance provided in Section V for the system shown in Fig. 22 to size ANSI (Subsection B) and IEC (Subsection C) CTs. The generator is high-impedance grounded, so we do not have to consider ground faults on the low-voltage side. The relevant data used for CT sizing are shown in Table IV. For Subsection B (ANSI), we assume that the system is 60 Hz, whereas for Subsection C (IEC), we assume that the system is 50 Hz. The negligible burden from digital relays is ignored.

Note that instead of 87T, if an overall differential was applied to protect both the generator and GSU transformer, the CT requirements would be lower and the setting process would be even simpler since we would only have to consider external faults at location F2.

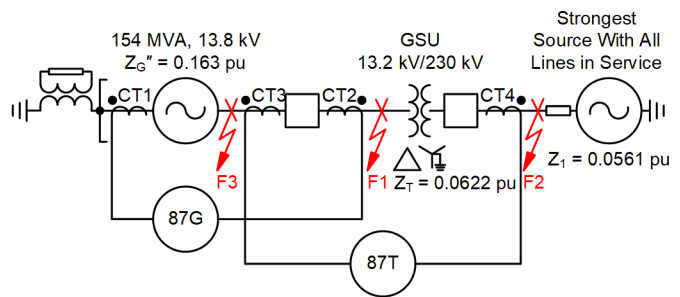


Fig. 22. Example System Used to Demonstrate CT Sizing With All Impedances Referenced to the Generator Ratings

TABLE IV  
USEFUL DATA FOR CT SELECTION

Parameter	Data
Rated current of generator/GSU transformer (including 50% margin [1])	9,664/555 A
Generator current for 3P fault at F1	39,530 A
GSU current for 3P fault at F2	28,610/1,642 A
Generator and GSU transformer current for single-line-to-ground (SLG) fault at F2	21,770/2,164 A
GSU transformer current for 3P fault at F3 with strongest system connected and all lines in service	54,460/3,126 A

### B. ANSI CT Sizing

As shown in Section V, Subsection B, and repeated here for convenience, the general equation used to size an ANSI CT is shown in (18), where  $I_F$  is the fault current and  $V_{ANSI}$  is defined at the CT terminals.  $K_{S\_MIN}$  is 1.8, per Fig. 20.

$$V_{ANSI} = K_{REM} \cdot K_{S\_MIN} \cdot \left( \frac{I_F}{N} \right) \cdot R_B \quad (18)$$

Based on the discussion of Section II, Subsection F,  $K_{REM} = 3$ . If during CT selection, a data sheet indicates a higher level of remanence, we may decide to choose a bigger CT or opt for a different one. Note that the C rating of the CT must be greater than both  $V_{ANSI}$  and C100 (Section V, Subsection III).

Once the ANSI voltage rating has been approximated, we look at a few data sheets. At this time, the  $R_{CT}$  will become available along with the excitation curve. For the ANSI example, we use an  $R_{CT}$  of 2.5 mΩ per turn and assume the lack of an excitation curve. Hence, we compare (19) with (20) to determine the level of CT over-dimensioning.

$$V_{SAT} = (K_{REM} \cdot K_S) \cdot \left( \frac{I_F}{N} \right) \cdot (R_B + R_{CT}) \quad (19)$$

$$V_{SAT\_CT} = V_{ANSI} + 20 \cdot I_{NOM} \cdot R_{CT} \quad (20)$$

Due to the over-dimensioning, the effective saturation factor ( $K_{S\_EFF}$ ) for the CT can be found via (21) allowing a more relaxed 87SLP2 setting to be obtained via use of Fig. 20.

$$K_{S\_EFF} = \left( \frac{V_{SAT\_CT}}{V_{SAT}} \right) \cdot K_{S\_MIN} \quad (21)$$

If different CTs comprising a differential zone have different  $V_{SAT\_CT}$  factors, the 87SLP2 setting for the zone is chosen by

considering the lowest  $K_{S\_EFF}$  via (22) and then referring to the 60 Hz curve in Fig. 20.

$$K_{S\_EFF\_87} = \min(K_{S\_EFF\_CT1}, K_{S\_EFF\_CT2} \dots K_{S\_EFF\_CTN}) \quad (22)$$

For this example, we assume 300 feet of 10AWG wire at 75°C. This gives a one-way lead resistance ( $R_{LEAD}$ ) of approximately 0.372  $\Omega$ . Note that  $R_B$  for a 3P fault equals  $R_{LEAD}$ , but for an SLG fault it equals  $2 \cdot R_{LEAD}$  [1].

### 1) CT1 and CT2 (87G)

Since the maximum current is 9,664 A, we choose a CT ratio of 10000:5. For CT1 and CT2, the worst-case external fault is a 3P fault at F1. Applying (18), we get (23).

$$V_{ANSI} = 3 \cdot 1.8 \cdot \left( \frac{39,530 \text{ A}}{2,000} \right) \cdot 0.372 \Omega = 39.7 \text{ V} \quad (23)$$

The CT must have an ANSI voltage rating higher than 39.7. A C100 CT may be applied. Once  $R_{CT}$  is available, we confirm that the saturation voltage is reasonable via (24) and (25).

$$V_{SAT} = 3 \cdot 1.8 \cdot \left( \frac{39,530 \text{ A}}{2,000} \right) \cdot (0.372 \Omega + 5 \Omega) = 573.3 \text{ V} \quad (24)$$

$$V_{SAT\_CT} = 100 \text{ V} + 20 \cdot 5 \text{ A} \cdot 5 \Omega = 600 \text{ V} \quad (25)$$

While a C100 CT is indeed adequate, at this stage we may apply engineering margins and use a C400 CT to obtain a  $V_{SAT\_CT}$  of 900 V instead. Additional considerations include the fact that an ANSI CT rated lower than C400 may not be easily available at such high CT ratios. Applying (21) using the parameters, we get (26).

$$K_{S\_EFF} = \left( \frac{900 \text{ V}}{573.3 \text{ V}} \right) \cdot 1.8 = 2.83 \quad (26)$$

Since both CTs comprising the 87G zone are the same, we refer to Fig. 20 to obtain an 87SLP2 higher than 79 percent for a  $K_{S\_EFF}$  of 2.83.

### 2) CT3 (87T)

CT3 has the same CT ratio as CT1 and CT2 because it carries the same load current. The GSU transformer winding connection does not allow CT3 to see zero-sequence current, so we only need to consider phase faults. The worst-case external phase fault current is the 3P fault at F3. Applying (18) gives us (27).

$$V_{ANSI} = 3 \cdot 1.8 \cdot \left( \frac{54,460 \text{ A}}{2,000} \right) \cdot 0.372 \Omega = 54.7 \text{ V} \quad (27)$$

We consider a C100 CT for this application. However, we notice that the worst-case saturation voltage calculated via (28) may be higher than what the C100 CT can provide, as calculated by (29). This is because the high fault current contribution from the system seen by CT3 makes the effective current 29.4 times nominal ( $3 \cdot 1.8 \cdot 5.45 \text{ pu}$ ) instead of the 20 times used by the CT manufacturer.

$$V_{SAT} = 3 \cdot 1.8 \cdot \left( \frac{54,460 \text{ A}}{2,000} \right) \cdot (0.372 \Omega + 5 \Omega) = 789.9 \text{ V} \quad (28)$$

$$V_{SAT\_CT} = 100 \text{ V} + 20 \cdot 5 \text{ A} \cdot 5 \Omega = 600 \text{ V} \quad (29)$$

If we apply a C400 CT for this application, we get a  $V_{SAT\_CT}$  of 900 V, which is sufficiently large. We apply (21) to get an effective  $K_S$ , as shown in (30).

$$K_{S\_EFF\_CT3} = \left( \frac{900 \text{ V}}{789.9 \text{ V}} \right) \cdot 1.8 = 2.05 \quad (30)$$

An alternative option is to increase the CT ratio to get an effective current of less than 20 times nominal. For instance, selecting a CT ratio of 3,000 while keeping  $R_{CT} = 5 \Omega$  reduces  $V_{SAT}$  in (28) to 526.6 V, lower than the  $V_{SAT\_CT}$  of 600 V in (29) and thus permitting application of a C100 CT.

### 3) CT4 (87T)

Since the maximum current on the high-voltage side is 555 A, we choose a CT ratio of 600:5. The worst-case external 3P fault is at F3 and the worst-case SLG fault is at F2. Applying (18), we get (31) and (32).

$$V_{ANSI\_3P} = 3 \cdot 1.8 \cdot \left( \frac{3,126 \text{ A}}{120} \right) \cdot 0.372 \Omega = 52.3 \text{ V} \quad (31)$$

$$V_{ANSI\_SLG} = 3 \cdot 1.8 \cdot \left( \frac{2,164 \text{ A}}{120} \right) \cdot (2 \cdot 0.372 \Omega) = 72.4 \text{ V} \quad (32)$$

The CT must have a voltage rating higher than 72.4 V. An ANSI CT with a rating of C100 is adequate for this application. Once  $R_{CT}$  is available, we apply (33), (34), and (35) to confirm that a C100 CT is adequate.

$$V_{SAT\_3P} = 3 \cdot 1.8 \cdot \left( \frac{3,126 \text{ A}}{120} \right) \cdot (0.372 \Omega + 0.3 \Omega) = 94.5 \text{ V} \quad (33)$$

$$V_{SAT\_SLG} = 3 \cdot 1.8 \cdot \left( \frac{2,164 \text{ A}}{120} \right) \cdot (2 \cdot 0.372 \Omega + 0.3 \Omega) = 101.7 \text{ V} \quad (34)$$

$$V_{SAT\_CT} = 100 \text{ V} + 20 \cdot 5 \text{ A} \cdot 0.3 \Omega = 130 \text{ V} \quad (35)$$

The level of CT over-dimensioning is calculated via (36).

$$K_{S\_EFF\_CT4} = \left( \frac{130 \text{ V}}{101.7 \text{ V}} \right) \cdot 1.8 = 2.3 \quad (36)$$

For the 87T application employing CT3 and CT4, we get an overall dimensioning per (22), as shown in (37).

$$K_{S\_EFF\_87T} = \min(2.05, 2.30) = 2.05 \quad (37)$$

Referring to Fig. 20 for a  $K_S$  of 2.05, we get an 87SLP2 setting for 87T higher than 86 percent.

The ANSI CT and settings required for this application are summarized in Table V. Note that for the calculations above,  $R_{CT}$  and  $V_{SAT\_CT}$  from the CT data sheet should be used, if available.

TABLE V  
CT REQUIREMENTS AND SETTINGS FOR ANSI EXAMPLE

	Minimum CT Requirement	87SLP2
CT1 and CT2 (87G)	10000:5 C400	79%
CT3 (87T)	10000:5 C400	86%
CT4 (87T)	600:5 C100	

### C. IEC CT Sizing

Although the definitions of the three approaches (P/PR vs. PX/PXR vs. TPX/TPY/TPZ) are different, they all have emf calculations that are comparable with each other [2]. We show an  $E_{AL}$  calculation that can be applied to P/PR and TPX/TPY/TPZ directly. For conversions to PX/PXR, if running into dimensioning challenges, divide  $E_{AL}$  by 1.25 to obtain the equivalent knee voltage for dimensioning [2].

The VA rating of the CT can be calculated via (38). Since the CT nominal current ( $I_{NOM\_CT}$ ) is 1 A, a minimum VA rating of 5 may be used according to Section V, Subsection B.

$$VA = I_{NOM\_CT}^2 \cdot R_{LEAD} \quad (38)$$

We size a Class P CT and assume  $K_{REM} = 5$ , per Section II, Subsection F. The general equation used to size the IEC CT is shown in (39).

$$E_{AL} = K_{REM} \cdot K_{TD\_MIN} \cdot \left(\frac{I_F}{N}\right) \cdot (R_B + R_{CT}) \quad (39)$$

The ALF for the Class P CT can then be calculated according to (40).

$$ALF = \frac{E_{AL}}{\left(\frac{VA}{I_{NOM\_CT}}\right) + (I_{NOM\_CT} \cdot R_{CT})} \quad (40)$$

Note that the ALF for the CT ( $ALF_{CT}$ ) must be greater than the ALF calculated per (40) but also larger than 20, per Section V, Subsection III. Due to the additional CT dimensioning, the effective saturation factor ( $K_{TD\_EFF}$ ) for the CT can be found via (41), allowing a more relaxed 87SLP2 setting to be obtained by referring to the 50 Hz curve in Fig. 20.

$$K_{TD\_EFF} = \left(\frac{ALF_{CT}}{ALF}\right) \cdot K_{TD\_MIN} \quad (41)$$

If different CTs comprising a differential zone have different ALF values, the 87SLP2 setting for the zone is chosen by considering the lowest  $K_{TD\_EFF}$  via (42).

$$K_{TD\_EFF\_87} = \min(K_{TD\_EFF\_CT1}, K_{TD\_EFF\_CT2}, \dots, K_{TD\_EFF\_CTN}) \quad (42)$$

For this example, we assume 100 m of 2.5 mm<sup>2</sup> wire at 75°C. This gives a one-way lead resistance ( $R_{LEAD}$ ) of approximately 0.841 Ω. Note that  $R_B$  for a 3P fault equals  $R_{LEAD}$ , but for an SLG fault equals  $2 \cdot R_{LEAD}$  [2]. Since this is a 1 A, 50 Hz CT, we assume a CT winding resistance of 6 mΩ per turn.

#### 1) CT1 and CT2 (87G)

Since the maximum current is 9,664 A, we choose a CT ratio of 10000:1. Based on (38), the VA rating can be calculated via (43).

$$VA = I^2 \cdot 0.841 = 0.841 \quad (43)$$

A minimum VA of 2.5 is chosen. The worst-case external fault is at F1. The  $E_{AL}$  per (39) can be found via (44).

$$E_{AL} = 5 \cdot 1.6 \cdot \left(\frac{39,530 \text{ A}}{10,000}\right) \cdot (0.841 \Omega + 60 \Omega) = 1,924 \text{ V} \quad (44)$$

The ALF calculation, per (40), is shown in (45).

$$ALF = \frac{1,924 \text{ V}}{2.5 + 60} = 30.78 \quad (45)$$

Choosing the next-highest ALF, we choose a 2.5 VA 5P 40 CT for this application. The effective  $K_{TD}$  is shown via (46).

$$K_{TD\_EFF\_87G} = \left(\frac{40}{30.78}\right) \cdot 1.6 = 2.08 \quad (46)$$

We look at Fig. 20 for an 87SLP2 of 83 percent.

#### 2) CT3 (87T)

CT3 has the same CT ratio as CT1 and CT2 because it carries the same load current. It also has the same VA rating since we assume the same burden in this example. The GSU transformer winding connection does not allow CT3 to see zero-sequence current. The worst-case fault current is the 3P fault at F3. The  $E_{AL}$  and ALF can be found via (47) and (48).

$$E_{AL} = 5 \cdot 1.6 \cdot \left(\frac{54,460 \text{ A}}{10,000}\right) \cdot (0.841 \Omega + 60 \Omega) = 2,651 \text{ V} \quad (47)$$

$$ALF = \frac{2,651 \text{ V}}{2.5 \text{ V} + 60 \text{ V}} = 42.41 \quad (48)$$

A 2.5 VA 5P 50 CT is adequate for this application. We get an effective  $K_{TD}$  via (49).

$$K_{TD\_EFF\_CT3} = \left(\frac{50}{42.41}\right) \cdot 1.6 = 1.89 \quad (49)$$

#### 3) CT4 (87T)

Since the maximum rated current on the high-voltage side is 555 A, we choose a CT ratio of 600:1. The VA rating can be calculated using (50).

$$VA = I^2 \cdot 0.841 = 0.841 \quad (50)$$

A minimum VA of 2.5 is chosen. The worst-case 3P external fault and SLG fault are at F2. The  $E_{AL}$  for both fault types and the ALF can be found via (51), (52), and (53).

$$E_{AL\_3P} = 5 \cdot 1.6 \cdot \left(\frac{3,126 \text{ A}}{600}\right) \cdot (0.841 \Omega + 3.6 \Omega) = 185.1 \text{ V} \quad (51)$$

$$E_{AL\_SLG} = 5 \cdot 1.6 \cdot \left(\frac{2,164 \text{ A}}{600}\right) \cdot (2 \cdot 0.841 \Omega + 3.6 \Omega) = 152.4 \text{ V} \quad (52)$$

$$ALF = \frac{185.1 \text{ V}}{2.5 + 3.6} = 30.3 \quad (53)$$

A 2.5VA 5P 40 CT may be used for this application. We get the effective  $K_{TD}$  shown in (54).

$$K_{TD\_EFF\_CT4} = \left(\frac{40}{30.3}\right) \cdot 1.6 = 2.1 \quad (54)$$

For the 87T application employing CT3 and CT4, we get the overall over-dimensioning shown in (55).

$$K_{TD\_EFF\_87T} = \min(1.89, 2.1) = 1.89 \quad (55)$$

Referring to Fig. 20 for a  $K_{TD}$  of 1.89, we get an 87SLP2 setting for 87T higher than 85 percent.

The IEC CT and settings required for this application are summarized in Table VI. Note that for the above calculations,  $R_{CT}$  from the CT data sheet should be used.

TABLE VI  
CT REQUIREMENTS AND SETTINGS FOR IEC EXAMPLE

	Minimum CT Requirement	87SLP2
CT1 and CT2 (87G)	10000:1 2.5 VA 5P 40	83%
CT3 (87T)	10000:1 2.5 VA 5P 50	85%
CT4 (87T)	600:1 2.5 VA 5P 40	

#### D. Summary

If we consider (32) and attempted to avoid CT saturation near a generating plant by considering the dc offset transient and remanence of 67 percent [1], we would obtain a value of 2,455 V (system X/R = 60) instead of the 72.4 V shown. Modern relays have sophisticated algorithms that can drastically relax CT requirements while remaining secure.

#### VIII. REFERENCES

- [1] IEEE C37.110-2007, IEEE Guide for the Application of Current Transformers Used for Protective Relaying Purposes.
- [2] IEC TR 61869-100:2017, Guidance for Application of Current Transformers in Power System Protection.
- [3] IEEE Power System Relaying and Control Committee, "CT Saturation Theory and Calculator," 2003. Available: <http://www.pes-psrc.org/kb/published/reports.html>.
- [4] A. R. van C. Warrington, *Protective Relays: Their Theory and Practice, Volume Two*, Chapman and Hall, 1969.
- [5] B. Kasztenny and D. Finney, "Generator Protection and CT Saturation Problems and Solutions," proceedings of the 58th Annual Conference for Protective Relay Engineers, College Station, TX, April 2005.
- [6] G. Benmouyal and S. E. Zocholl, "The Impact of High Fault Current and CT Rating Limits on Overcurrent Protection," proceedings of the 29th Annual Western Protective Relay Conference, Spokane, WA, October 2002.
- [7] H. J. Altuve, N. Fischer, G. Benmouyal, and D. Finney, "Sizing Current Transformers for Line Protection Applications," proceedings of the 66th Annual Conference for Protective Relay Engineers, College Station, TX, April 2013.
- [8] R. G. Bruce and A. Wright, "Remanent Flux in Current-Transformer Cores," *Proceedings of the Institution of Electrical Engineers*, Vol. 113, Issue 5, May 1966, pp. 915–920.
- [9] K. Barner, N. Klingerman, M. Thompson, R. Chowdhury, D. Finney, and S. Samineni, "OOPS, Out of Phase Synchronization," proceedings of the 73rd Annual Georgia Tech Protective Relaying Conference, Atlanta, GA, May 2019.
- [10] IEEE PSRC, "Gapped Core Current Transformer Characteristics and Performance," *IEEE Transactions on Power Delivery*, Vol. 5, Issue 4, October 1990, pp. 1,732–1,740.
- [11] S. E. Zocholl and D. W. Smaha, "Current Transformer Concepts," proceedings of the 46th Annual Georgia Tech Protective Relaying Conference, Atlanta, GA, April 1992.
- [12] R. Garrett, W. C. Kotheimer, and S. E. Zocholl, "Computer Simulation of Current Transformers and Relays for Performance Analysis," proceedings of 14th Annual Western Protective Relay Conference, Spokane, WA, October 1988.
- [13] *Real Time Digital Simulator - Power System User's Manual, Section 7.2: Current Transformers*, RTDS Technologies, Inc., Winnipeg, Canada, December 2013.
- [14] W. L. A. Neves and H. W. Dommel, "On Modelling Iron Core Nonlinearities," *IEEE Transactions on Power Systems*, Vol. 8, Issue 2, May 1993, pp. 417–425.
- [15] *CT Analyzer User Manual*. 2016. Available: [http://userequip.com/files/specs/6031/CT-Analyzer\\_user%20manual.pdf](http://userequip.com/files/specs/6031/CT-Analyzer_user%20manual.pdf).

- [16] M. Thompson, R. Folkers, and A. Sinclair, "Secure Application of Transformer Differential Relays for Bus Protection," proceedings of 58th Annual Conference for Protective Relay Engineers, College Station, TX, April 2005.
- [17] B. Kasztenny, D. Taylor, and N. Fischer, "Impact of Geomagnetically Induced Currents on Protection Current Transformers," proceedings of the 13th International Conference on Developments in Power System Protection, Edinburgh, UK, March 2016.
- [18] M. J. Thompson, "Percentage Restrained Differential, Percentage of What?" proceedings of the 64th Annual Conference for Protective Relay Engineers, College Station, TX, April 2011.
- [19] B. Kasztenny, M. J. Thompson, and D. Taylor, "Time-Domain Elements Optimize the Security and Performance of Transformer Protection," proceedings of 71st Annual Conference for Protective Relay Engineers, College Station, TX, March 2018.
- [20] A. Hargrave, M. Thompson, and B. Heilman, "Beyond the Knee Point: A Practical Guide to CT Saturation," proceedings of 71st Annual Conference for Protective Relay Engineers, College Station, TX, March 2018.

#### IX. BIOGRAPHIES

**Ritwik Chowdhury** received his bachelor of engineering degree from the University of British Columbia and his master of engineering degree from the University of Toronto. He joined Schweitzer Engineering Laboratories, Inc. in 2012, where he has worked as an application engineer and presently works as a lead power engineer. Ritwik holds 2 patents and has authored over 10 technical papers in the area of power system protection and controlled switching. He is an active contributor to IEEE PSRC committee standards development, a member of the rotating machinery subcommittee, and a registered professional engineer in the province of Ontario.

**Dale Finney** received his bachelor of engineering degree from Lakehead University and his master of engineering degree from the University of Toronto. He began his career with Ontario Hydro, where he worked as a protection and control engineer. Currently, Mr. Finney is employed as a principal power engineer with Schweitzer Engineering Laboratories, Inc. Mr. Finney holds more than 10 patents and has authored more than 30 papers in the area of power system protection. He is a member of the main committee and chair of the rotating machinery subcommittee of the IEEE PSRC committee. He is a senior member of the IEEE and a registered professional engineer in the province of Nova Scotia.

**Normann Fischer** received a Higher Diploma in Technology, with honors, from Technikon Witwatersrand, Johannesburg, South Africa, in 1988; a BSEE, with honors, from the University of Cape Town in 1993; an MSEE from the University of Idaho in 2005; and a PhD from the University of Idaho in 2014. He joined Eskom as a protection technician in 1984 and was a senior design engineer in the Eskom protection design department for three years. He then joined IST Energy as a senior design engineer in 1996. In 1999, Normann joined Schweitzer Engineering Laboratories, Inc., where he is currently a fellow engineer in the Research and Development division. He was a registered professional engineer in South Africa and a member of the South African Institute of Electrical Engineers. He is currently a senior member of IEEE and a member of the American Society for Engineering Education (ASEE). Normann has authored over 60 technical and 10 transaction papers and holds over 20 patents related to electrical engineering and power system protection.

**Douglas Taylor** received his BSEE and MSEE degrees from the University of Idaho in 2007 and 2009. He joined Schweitzer Engineering Laboratories, Inc. in 2009 and worked as a protection engineer and as a research engineer in the Research and Development division. Currently, Doug is working as a protection engineer at Avista Utilities. He is a registered professional engineer in the state of Washington and is a member of the IEEE. His main interests are power system protection and power system analysis. Doug holds 3 patents and has helped author more than 15 technical papers in the area of power system protection.